# REPORT DOCUMENTATION PAGE

Form Approved OMB NO. 0704-0188



| 1. REPORT DATE (DD-MM-YYYY) | 2. REPORT TYPE | 3. DATES COVERED (From - To) |
|---|---|---|
| 08-02-2017 | Final Report | 15-Sep-2012 - 14-Sep-2016 |

**4. TITLE AND SUBTITLE**
Final Report: Reducing False Alarms in Ion Mobility Spectrometry Detectors - Determination of Accurate and Precise Ion Mobility Spectrometry Constants

**5a. CONTRACT NUMBER**
W911NF-12-1-0575

**5b. GRANT NUMBER**

**5c. PROGRAM ELEMENT NUMBER**
611102

**6. AUTHORS**
Brian C. Hauck, William F. Siems, Charles S. Harden, Vincent M. McHugh, Herbert H. Hill Jr.

**5d. PROJECT NUMBER**

**5e. TASK NUMBER**

**5f. WORK UNIT NUMBER**

**7. PERFORMING ORGANIZATION NAMES AND ADDRESSES**
Washington State University
423 Neill Hall

Pullman, WA 99164 -3140

**8. PERFORMING ORGANIZATION REPORT NUMBER**

**9. SPONSORING/MONITORING AGENCY NAME(S) AND ADDRESS (ES)**
U.S. Army Research Office
P.O. Box 12211
Research Triangle Park, NC 27709-2211

**10. SPONSOR/MONITOR'S ACRONYM(S)**
ARO

**11. SPONSOR/MONITOR'S REPORT NUMBER(S)**
62620-CH.5

**12. DISTRIBUTION AVAILIBILITY STATEMENT**
Approved for Public Release; Distribution Unlimited

**13. SUPPLEMENTARY NOTES**
The views, opinions and/or findings contained in this report are those of the author(s) and should not contrued as an official Department of the Army position, policy or decision, unless so designated by other documentation.

**14. ABSTRACT**
Ion mobility spectrometry (IMS) is a widely used analytical technique for detecting chemical warfare agents, narcotics, and explosives in the field. Detection of a compound of interest is based on the ion's reduced mobility (K0) value. The detection windows for compounds of interest are currently only as small as ± 2% of the predicted drift time measurement for the compound of interest, resulting in false positive alarms when an interferent appears within these wide detection windows. Accurate K0 values that are an order of magnitude better than the current literature values will lower the propagation of error when predicting the drift time of an ion and reduce the width of

**15. SUBJECT TERMS**
Ion Mobility Spectrometry, Accuracy, Precision, False Alarms, Explosives

| 16. SECURITY CLASSIFICATION OF: | | | 17. LIMITATION OF ABSTRACT | 15. NUMBER OF PAGES | 19a. NAME OF RESPONSIBLE PERSON |
|---|---|---|---|---|---|
| a. REPORT | b. ABSTRACT | c. THIS PAGE | | | Herbert Hill, Jr. |
| UU | UU | UU | UU | | 19b. TELEPHONE NUMBER: 509-595-1492 |

## Report Title

Final Report: Reducing False Alarms in Ion Mobility Spectrometry Detectors - Determination of Accurate and Precise Ion Mobility Spectrometry Constants


## ABSTRACT

Ion mobility spectrometry (IMS) is a widely used analytical technique for detecting chemical warfare agents, narcotics, and explosives in the field. Detection of a compound of interest is based on the ion's reduced mobility (K0) value. The detection windows for compounds of interest are currently only as small as ± 2% of the predicted drift time measurement for the compound of interest, resulting in false positive alarms when an interferent appears within these wide detection windows. Accurate K0 values that are an order of magnitude better than the current literature values will lower the propagation of error when predicting the drift time of an ion and reduce the width of the detection windows. An accurate IMS instrument has been constructed and installed on an existing time-of-flight mass spectrometer (tofMS) and accurate K0 values of selected compounds have been measured as a function of multiple instrumental parameters. This initial database of accurate K0 values will be expanded upon in the future to include additional compounds of interest. The database of accurate K0 values will be used to calibrate IMS-based field instruments and reduce their rates of false positive alarms without increasing their rates of false negative responses or changing their hardware.


---

## Enter List of papers submitted or published that acknowledge ARO support from the start of the project to the date of this printing. List the papers, including journal references, in the following categories:

### (a) Papers published in peer-reviewed journals (N/A for none)

| Received | | Paper |
|---|---|---|
| 01/12/2017 | 3 | Brian C. Hauck, William F. Siems, Charles S. Harden, Vincent M. McHugh, Herbert H. Hill. E/N effects on K0 values revealed by high precision measurements under low field conditions, Review of Scientific Instruments, ( ): 075104. doi: |
| **TOTAL:** | **1** | |

**Number of Papers published in peer-reviewed journals:**

---

### (b) Papers published in non-peer-reviewed journals (N/A for none)

| Received | | Paper |
|---|---|---|
| **TOTAL:** | | |

**Number of Papers published in non peer-reviewed journals:**

## (c) Presentations

Brian C. Hauck, William F. Siems, Charles S. Harden, Vincent M. McHugh, Herbert H. Hill, Jr. Accurate Ion Mobility Spectrometry: High Resolution Without Reduction in Sensitivity - Building the Database 24th International Conference on Ion Mobility Spectrometry; Córdoba, Spain; July 26- July 30, 2015.

William F. Siems, Brian C. Hauck, Charles S. Harden, Vincent M. McHugh, Herbert H. Hill, Jr. One More Significant Figure for K0 – How Difficult Can That Be? 24th International Conference on Ion Mobility Spectrometry; Córdoba, Spain; July 26- July 30, 2015.

Brian C. Hauck, William F. Siems, Charles S. Harden, Vincent M. McHugh, Herbert H. Hill, Jr. Accurate Ion Mobility Spectrometry: High Resolution Without Reduction in Sensitivity - Building the Database 7th Annual Workshop on Trace Explosives Detection; Pittsburgh, Pennsylvania; April 27 - May 1, 2015.

Brian C. Hauck, William F. Siems, Charles S. Harden, Vincent M. McHugh, Herbert H. Hill, Jr. Accurate Ion Mobility Spectrometry: Building the Database Pittcon Conference & Expo 2015; New Orleans, Louisiana; March 8-12, 2015.

Brian C. Hauck, William F. Siems, Charles S. Harden, Vincent M. McHugh, Herbert H. Hill, Jr. Accurate Ion Mobility Spectrometry in National Security: Validation of Instrumental Parameters and Initial Results 23rd International Conference on Ion Mobility Spectrometry; Asheville, North Carolina; July 27-August 1, 2014.

Brian C. Hauck, William F. Siems, Charles S. Harden, Vincent M. McHugh, Herbert H. Hill, Jr. Accurate Ion Mobility Spectrometry: Requirements and Results 62nd ASMS Conference on Mass Spectrometry and Allied Topics; Baltimore, Maryland; June 15-19, 2014.

Brian C. Hauck, William F. Siems, Charles S. Harden, Vincent M. McHugh, Herbert H. Hill, Jr. Accurate Ion Mobility Spectrometry: Technical Specifications 62nd ASMS Conference on Mass Spectrometry and Allied Topics; Baltimore, Maryland; June 15-19, 2014.

Brian C. Hauck, William F. Siems, Charles S. Harden, Vincent M. McHugh, Herbert H. Hill, Jr. Accurate Ion Mobility Spectrometry: Requirements and Results 6th Annual Workshop on Trace Explosives Detection; Charlottesville, Virginia; April 7-11, 2014.

Brian C. Hauck, William F. Siems, Charles S. Harden, Vincent M. McHugh, Herbert H. Hill, Jr. Accurate Ion Mobility Spectrometer 22nd International Conference on Ion Mobility Spectrometry; Boppard, Germany; July 20-26, 2013.

**Number of Presentations:** 9.00

## Non Peer-Reviewed Conference Proceeding publications (other than abstracts):

Received Paper

**TOTAL:**

**Number of Non Peer-Reviewed Conference Proceeding publications (other than abstracts):**

## Peer-Reviewed Conference Proceeding publications (other than abstracts):

Received Paper

**TOTAL:**

**Number of Peer-Reviewed Conference Proceeding publications (other than abstracts):**

## (d) Manuscripts

Received Paper

**TOTAL:**

**Number of Manuscripts:**

## Books

Received Book

**TOTAL:**

| Received | Book Chapter |
|---|---|

**TOTAL:**

## Patents Submitted

## Patents Awarded

## Awards

Student Travel Award, Trace Explosives Detection Workshop, Pittsburgh, PA (2015)

## Graduate Students

| NAME | PERCENT_SUPPORTED | Discipline |
|---|---|---|
| Brian C. Hauck | 0.50 | |
| **FTE Equivalent:** | **0.50** | |
| **Total Number:** | **1** | |

## Names of Post Doctorates

| NAME | PERCENT_SUPPORTED |
|---|---|
| **FTE Equivalent:** | |
| **Total Number:** | |

## Names of Faculty Supported

| NAME | PERCENT_SUPPORTED |
|---|---|
| **FTE Equivalent:** | |
| **Total Number:** | |

## Names of Under Graduate students supported

| NAME | PERCENT_SUPPORTED |
|---|---|
| **FTE Equivalent:** | |
| **Total Number:** | |

## Student Metrics

This section only applies to graduating undergraduates supported by this agreement in this reporting period

The number of undergraduates funded by this agreement who graduated during this period: ..... 0.00

The number of undergraduates funded by this agreement who graduated during this period with a degree in science, mathematics, engineering, or technology fields:..... 0.00

The number of undergraduates funded by your agreement who graduated during this period and will continue to pursue a graduate or Ph.D. degree in science, mathematics, engineering, or technology fields:..... 0.00

Number of graduating undergraduates who achieved a 3.5 GPA to 4.0 (4.0 max scale):..... 0.00

Number of graduating undergraduates funded by a DoD funded Center of Excellence grant for Education, Research and Engineering:..... 0.00

The number of undergraduates funded by your agreement who graduated during this period and intend to work for the Department of Defense ..... 0.00

The number of undergraduates funded by your agreement who graduated during this period and will receive scholarships or fellowships for further studies in science, mathematics, engineering or technology fields:..... 0.00

## Names of Personnel receiving masters degrees

| NAME |
|---|
| **Total Number:** |

## Names of personnel receiving PHDs

| NAME |
|---|
| Brian C. Hauck |
| **Total Number:** 1 |

## Names of other research staff

| NAME | PERCENT_SUPPORTED |
|---|---|
| **FTE Equivalent:** | |
| **Total Number:** | |

## Sub Contractors (DD882)

## Inventions (DD882)

## Scientific Progress

See Attachment

## Technology Transfer

Accurate ion mobility - time of flight mass spectrometer developed at Washington State University transferred to Edgewood Chemical Biological Center for permanent installation on site.

# Final Report
# Reducing False Alarms in Ion Mobility Spectrometry Detectors – Determination of Accurate and Precise Ion Mobility Spectrometry Constants

## Final Report for US Army/ECBC Proposal # *62620-CH*
## *Agreement # W911NF-12-1-0575*

**Submitted to:**

**Dr. Dawanne Poree**
**ARO Program Manager and COR**
**Army Research Office**
**Research Triangle Park, NC 27709**

**Submitted by:**

**Dr. Brian C. Hauck***
**Dr. Herbert H. Hill, Jr.**
**Department of Chemistry**
**PO BOX 644630**
**Washington State University**
**Pullman, WA 99164-4630**

**Tel: (509) 335-5648**
**Email: hhhill@wsu.edu**

**September 15, 2012 – September 14, 2016**

***Current affiliation:**
**ORISE Postdoctoral Fellow**
**Detection Spectrometry Branch**
**U.S. Army Edgewood Chemical Biological Center**
**Aberdeen Proving Ground, MD 21010-5424**

**CC:**

**Dr. Mary M. Wade**
**Branch Chief Detection Spectrometry Branch**
**ATTN: RDCB-DRI-D U.S. Army Edgewood Chemical Biological Center**
**Aberdeen Proving Ground, MD 21010-5424**

**Matthew Michener**
**Grant and Contract Coordinator**
**WSU Office of Grants & Research Development**

## EXECUTIVE SUMMARY

Ion Mobility Spectrometry (IMS) is a gas-phase separation technique used by the U.S. Military and others for explosives and chemical warfare agent (CWA) detection. IMS-based field detection instruments suffer from false positive alarms due to wide detection windows that result from inaccurate reduced ion mobility ($K_0$) values. The overall goal of the work was two-fold:

- Construct an accurate IMS instrument capable of measuring $K_0$ values to an accuracy of ± 0.2% (± 0.002 $cm^2V^{-1}s^{-1}$) or better, an order of magnitude better than current capabilities
- Make accurate and precise experimental measurements of $K_0$ values for selected target chemicals

The objectives of the experimental work detailed in this report were to:

- Construct and hermetically seal an accurate IMS instrument
- Introduce, ionize, and analyze the following compounds by IMS
    - Ammonia reactant ion (positive ion mode active)
    - DMMP: dimethyl methylphosphonate (positive ion mode active)
    - TNT: 2,4,6-trinitrotoluene (negative ion mode active)
    - Tetryl: N-Methyl-N-(2,4,6-trinitrophenyl)nitramide (negative ion mode active)
    - PETN: 2,2-Bis[(nitrooxy)methyl]propane-1,3-diyl dinitrate (negative ion mode active)
- Obtain $K_0$ values for each of the above compounds at varying electric field strengths, drift gas water vapor concentration, and temperatures

Results of the Positive Mode Study

- The $K_0$ values of the DMMP monomer and ammonia reactant ion increased with increasing temperature
- The $K_0$ values of the DMMP monomer and ammonia reactant ion decreased with increasing drift gas water content
- The $K_0$ value of the DMMP dimer did not significantly change with either changing temperature or drift gas water content
- The $K_0$ values of all ions studied decreased with increasing electric field strength

Results of the Negative Mode Study:

- The $K_0$ values of all ions studied increased with increasing temperature
- The $K_0$ values of all ions studied decreased with increasing drift gas water content
- The $K_0$ values of all ions decreased with increasing electric field strength

The impact of the work will be to:

- Create an initial database of accurate $K_0$ values for the compounds of interest studied
- Enable the selection and evaluation of an appropriate mobility reference standard in order to calibrate IMS-based field instruments in real time
- Reduce the false positive alarm rates of IMS-based field instruments without increasing their rates of false negative responses
- Make these improvements to IMS-based field instruments using only software changes and without expending resources for hardware changes

## PUBLICATIONS UNDER ARO SPONSORSHIP DURING PROJECT PERIOD

*PUBLICATIONS (3 Total)*

1. Brian C. Hauck. High Accuracy Ion Mobility Spectrometry to Reduce False Alarm Rates in National Security. Ph.D. Thesis, Washington State University, 2016.

2. Brian C. Hauck, William F. Siems, Charles S. Harden, Vincent M. McHugh, Herbert H. Hill, Jr. ***E/N* effects on $K_0$ values revealed by high precision measurements under low field conditions**, *Review of Scientific Instruments*, **2016**, 87(7), 075104. doi: 10.1063/1.4955208

3. Brian C. Hauck, Eric J. Davis, Aurora E. Clark, William F. Siems, Charles S. Harden, Vincent M. McHugh, Herbert H. Hill, Jr. **Determining the water content of a drift gas using reduced mobility measurements**, *International Journal of Mass Spectrometry*, **2014**, 368, 37-44. doi: 10.1016/j.ijms.2014.05.010

*ORAL PRESENTATIONS (7 Total)*

1. Brian C. Hauck, William F. Siems, Charles S. Harden, Vincent M. McHugh, Herbert H. Hill, Jr. **Accurate Ion Mobility Spectrometry: High Resolution Without Reduction in Sensitivity - Building the Database** *24th International Conference on Ion Mobility Spectrometry*; Córdoba, Spain; July 26- July 30, 2015.

2. William F. Siems, Brian C. Hauck, Charles S. Harden, Vincent M. McHugh, Herbert H. Hill, Jr. **One More Significant Figure for $K_0$ – How Difficult Can That Be?** *24th International Conference on Ion Mobility Spectrometry*; Córdoba, Spain; July 26- July 30, 2015.

3. Brian C. Hauck, William F. Siems, Charles S. Harden, Vincent M. McHugh, Herbert H. Hill, Jr. **Accurate Ion Mobility Spectrometry: High Resolution Without Reduction in Sensitivity - Building the Database** *7th Annual Workshop on Trace Explosives Detection*; Pittsburgh, Pennsylvania; April 27 - May 1, 2015.

4. Brian C. Hauck, William F. Siems, Charles S. Harden, Vincent M. McHugh, Herbert H. Hill, Jr. **Accurate Ion Mobility Spectrometry: Building the Database** *Pittcon Conference & Expo 2015*; New Orleans, Louisiana; March 8-12, 2015.

5. Brian C. Hauck, William F. Siems, Charles S. Harden, Vincent M. McHugh, Herbert H. Hill, Jr. **Accurate Ion Mobility Spectrometry: Requirements and Results** *62nd ASMS Conference on Mass Spectrometry and Allied Topics*; Baltimore, Maryland; June 15-19, 2014.

6. Brian C. Hauck, William F. Siems, Charles S. Harden, Vincent M. McHugh, Herbert H. Hill, Jr. **Accurate Ion Mobility Spectrometry: Requirements and Results** *6th Annual Workshop on Trace Explosives Detection*; Charlottesville, Virginia; April 7-11, 2014.

7. Brian C. Hauck, William F. Siems, Charles S. Harden, Vincent M. McHugh, Herbert H. Hill, Jr. **Accurate Ion Mobility Spectrometer** *22nd International Conference on Ion Mobility Spectrometry*; Boppard, Germany; July 20-26, 2013.

*POSTER PRESENTATIONS (2 Total)*

1. Brian C. Hauck, William F. Siems, Charles S. Harden, Vincent M. McHugh, Herbert H. Hill, Jr. **Accurate Ion Mobility Spectrometry in National Security: Validation of Instrumental Parameters and Initial Results** *23rd International Conference on Ion Mobility Spectrometry*; Asheville, North Carolina; July 27-August 1, 2014.

2. Brian C. Hauck, William F. Siems, Charles S. Harden, Vincent M. McHugh, Herbert H. Hill, Jr. **Accurate Ion Mobility Spectrometry: Technical Specifications** *62nd ASMS Conference on Mass Spectrometry and Allied Topics*; Baltimore, Maryland; June 15-19, 2014.

## ABSTRACT

Ion mobility spectrometry (IMS) is a widely used analytical technique for detecting chemical warfare agents (CWA), narcotics, and explosives in the field. Detection of a compound of interest is based on the ion's reduced mobility ($K_0$) value. The detection windows for compounds of interest have historically been as small as ± 2% of the predicted drift time measurement for the compound of interest, resulting in false positive alarms when an interferent appears within these wide detection windows. Accurate $K_0$ values that are an order of magnitude better than the current literature values will lower the propagation of error when predicting the drift time of an ion and reduce the width of the detection windows. An accurate IMS instrument has been constructed and interfaced with an existing *time-of-flight* mass spectrometer (*tof*MS) and accurate $K_0$ values of selected compounds have been measured as a function of multiple instrumental parameters. This initial database of accurate $K_0$ values will be expanded in the future to include additional compounds of interest, namely CWA (toxic chemicals) and explosives. The database of accurate $K_0$ values will be used to calibrate IMS-based field instruments and reduce their rates of false positive alarms without increasing their rates of false negative responses or modifying hardware.

## INTRODUCTION

Ion mobility spectrometry (IMS) is the preferred analytical technique in the detection of chemical warfare agents (CWA), narcotics, and explosives within the realm of national security. Compounds of interest are identified using the ion's $K_0$ value, which is calculated based on the amount of time ($t_d$) it takes for the ion to drift a known length ($L$) under a weak electric field ($V$) applied across $L$ and is normalized to standard temperature ($T$) and pressure ($P$), as shown in Equation (1).[1]

$$K_0 = \frac{L^2}{V t_d}\left(\frac{273.15}{T}\right)\left(\frac{P}{760}\right) \quad (1)$$

A field instrument looks for a compound of interest, such as an explosive, by predicting the measured $t_d$ of the compound and establishing a detection window around that predicted $t_d$. The predicted $t_d$ is based on the instrumental parameters ($L$, $V$, $T$, and $P$) and the "known" $K_0$ values of the compound of interest ($K_{0\ cmpd}$) and an instrumental standard ($K_{0\ std}$). Both $K_0$ values used are at the specified instrumental and field parameters. This is shown in Equation (2) in which the product of the instrumental standard's $K_0$ value ($K_{0\ std}$) and its measured drift time ($t_{d\ std}$) on the field instrument is the instrument factor ($C_i$), sometimes referred to as an instrument constant, that takes all of the instrumental parameters into account for that unit. Because the product of a compound of interest's $K_0$ value ($K_{0\ cmpd}$) and its drift time ($t_{d\ cmpd}$) will also equal $C_i$, the variables relating to the reference standard and compound of interest may be arranged as in Equation (2) to predict $t_{d\ cmpd}$, which is specific for that instrument, from the measured $t_{d\ std}$ and the known values of $K_{0\ std}$ and $K_{0\ cmpd}$ from the available literature.[2-8]

$$\frac{(K_{0\ std})t_{d\ std}}{K_{0\ cmpd}} = \frac{C_i}{K_{0\ cmpd}} = t_{d\ cmpd} \quad (2)$$

Once $t_{d\ cmpd}$ has been predicted from $C_i$ and $K_{0\ cmpd}$, a detection window is set up around the predicted value of $t_{d\ cmpd}$ through the propagation of error in Equation (2). If a $t_d$ spectral peak falls within the window it is deemed a true positive response for the compound. The width of the detection window and the error in any predicted drift time has historically been, at best, accurate to ± 2%.[3,9] This results in false positive alarms whenever an interferent with a drift time within 2% of the predicted drift time falls within the detection window and causes the loss of time and money as resources are diverted to respond to the alarm. These detection windows also cannot be arbitrarily decreased because of the risk of excluding a true compound of interest peak from the detection window, resulting in a false negative response.

The only way to reduce the width of detection windows and improve specificity without inadvertently decreasing sensitivity is to increase the accuracy of $K_0$ values referenced by the field instruments when predicting a compound's drift time in Equation (2). In order to measure accurate $K_0$ values for compounds, each of the variables measured to produce the $K_0$ value; $L$, $V$, $t_d$, $P$, and $T$, need to be accurately and precisely measured and controlled so as to reduce the error that is propagated through the calculation of the $K_0$ values. After assembling a database of accurate $K_0$ values for the compounds of interest, including mobility reference standards and hazards, the values will be referenced by an improved detection algorithm program written for the IMS-based field instruments in order to calibrate them in real time.

The objective of this work has been to construct an accurate IMS instrument capable of measuring $K_0$ values to an accuracy of at least ± 0.2% (± 0.002 $cm^2V^{-1}s^{-1}$) or better. After completing the construction of the accurate instrument, selected compounds of interest were to be analyzed and accurate $K_0$ values obtained as a function of temperature, drift gas water content, and electric field. This report details the final results found for US Army/ ECBC Proposal #62620-CH,

Agreement #W911NF—12-1-0575 under the direction of WSU co-Principal Investigator Dr. Herbert H. Hill, Jr. The first half of the results detail the method of construction for the accurate IMS instrument and the equipment and procedures required to accurately and precisely control the five variables within Equation (1). These details and other scientific progress have also been previously published in the open literature.[10-12] The second half of this report presents the initial database of accurate $K_0$ values obtained for six ions studied and evaluates the trends found within the data.

## SCIENTIFIC PROGRESS AND ACCOMPLISHMENTS

### 1. Reduction of error

The degree of error in calculating $K_0$ values with the IMS instrument is dependent upon the measured accuracies of the components within the system as they relate to the five variables of Equation (1); length ($L$, cm), voltage ($V$, V), drift time ($t_d$, ms), temperature ($T$, K), and pressure ($P$, Torr). The potentials for error from each of these parameters were minimized by using the highest accuracy components and procedures, thereby reducing each variable's error in measurement and control.

#### *1.1 Length*

The length of the drift tube was defined as the distance between two sets of Bradbury-Nielson (BN) ion gate wires. The length between BN ion gates was calculated by taking the sum of three length measurements at room temperature; half of each gate and the length of the drift tube between both BN ion gates. The length was measured by a pair of 12 inch calipers from

Mitutoyo (Aurora, IL) with an error of ± 0.0015in (± 0.0381 mm). All length measurements were corrected for thermal expansion.

*1.2 Voltage*

Voltage was supplied to the drift tube by an LS020 reversible 20kV power supply from Exelis (West Springfield, MA). The power supply was capable of a 20kV maximum output and had a 1ppm output ripple. The electric field (*E*) within the IMS instrument was set up to be homogenous and adjustable from the first electrode to the inlet of the *tof*MS, with the electric field terminating at the same potential as the inlet of the *tof*MS. A series of 20MΩ resistors (Caddock Electronics Inc., Riverside, CA, ± 1%) were attached between electrode rings via pin connectors from Positronic Industries Inc. (Springfield, MO). A 5MΩ variable resistor (Newark, Chicago, IL) was attached as a potentiometer across the drift gas entry showerhead (SH) after the second BN ion gate, and a second series of 5MΩ variable resistors leading to ground were attached to the end of the resistor chain in order to establish the electric field. The electric field was set to the desired value by adjusting the voltage applied to the first ring ($V_s$) and the total resistance of the chain after the potentiometer. 10MΩ resistors (± 1%) from Caddock were also used across the first BN ion gate and leading up to the second BN ion gate reference instead of 20 MΩ resistors.

The voltage across the drift space was measured using an 8846A digital multimeter (DMM) from Fluke (Everett, WA). The DMM had an accuracy of ± 0.0024% of the measurement plus 0.0005% of the DMM range used. The DMM was coupled with a 10GΩ high precision HVP-250 voltage divider from Computer Power Supplies (Tigard, OR) with an accuracy of ± 0.05% over the full measurement. The divider had a ratio of 10,000:1 (measured directly to $1.003\times10^{-4} \pm 5\times10^{-}$

[7]) and required the DMM to be used in high input impedance mode when measuring voltage due to the resulting input voltage being less than 1 V.

The power supply had such a low output current that required the use of higher resistors in the electric field. However, because the 10 GΩ voltage divider had a comparatively high resistance to that of the total resistor chain on the IMS instrument, it offered the current running through the resistor chain an alternate path to ground of near equivalent resistance and drew down the observed voltage measurement when the probe was applied. This necessitated a correction to the measurement obtained from the DMM to determine the "true" voltage at the point of measurement point using Equation (5).

$$V_{true} = V_{meas}\left(\frac{\mathrm{II}R+R_{upstrm}}{\mathrm{II}R}\right)\left(\frac{R_{dwnstrm}}{R_T}\right)\left(\frac{1}{PDR}\right) \quad (5)$$

In Equation (5), $V_{true}$ is the true value of the voltage applied to the electrode, $V_{meas}$ is the voltage measured directly with the High Voltage (HV) probe and DMM, II*R* is the parallel resistance between the HV probe and the resistor chain downstream (towards ground) from the measurement point, $R_{upstrm}$ is the total value of the entire resistor chain upstream (towards the first electrode) from the measurement point, $R_{dwnstrm}$ is the value of the resistor chain downstream from the measurement point, $R_T$ is the value of the total resistor chain, and *PDR* is the value of the HV Probe Divider Ratio previously stated. The directly measured values of the resistors, as opposed to their nominal values, were used in Equation (5). The voltage difference between the first and second BN ion gate reference voltages was used in reduced mobility calculations to correspond with the length measured between BN ion gate wires.

The closure voltage at both BN ion gates was scaled with the electric field in order to maintain a homogenous electric field and to have ions pass through identical equipotential lines between BN ion gate wires for each electric field. To determine the minimum BN ion gate closure

voltage, the IMS instrument was operated in manual mode with the first BN ion gate closed at the lowest field. The BN ion gate closure voltage was slowly increased until no spectra appeared over the course of twenty minutes. This minimum BN ion gate closure voltage was then scaled for each successive electric field. When one BN ion gate was being operated to collect spectra, the other BN ion gate was connected to the resistor chain using wire and alligator clips in order to maintain the homogeneity of the electric field. The gate pulse width was maintained at 200 $\mu$s for all drift time measurements at both BN ion gates.

*1.3 Drift Time*

The *tof*MS was used to measure the drift time of all ions. Two separate drift times were recorded; the first drift time from the first BN ion gate and the second drift time measured from the second BN ion gate. The drift time between the two BN ion gates was determined by taking the difference between the two drift time measurements, and the time spent past the second BN ion gate and within the *tof*MS was thereby eliminated. In this manner the drift time measurement between the two BN ion gates directly corresponded with the measured length between the two BN ion gates. All $K_0$ values here used drift time measurements obtained in this IMS-MS mode in order to mass identify all product ions.

The IMS instrument also had the option of measuring the drift time in IMS standalone mode using a Faraday plate built into drift gas entry. When using the Faraday Plate, the first BN ion gate is used the same as in IMS-MS mode and the second BN ion gate is used as an aperture grid. Spectra for the Faraday plate can be obtained and analyzed using a LABVIEW program written in-house at WSU.[13]

*1.4 Temperature*

The IMS instrument was heated by two 25.5 cm long heater cartridges from Heatcon (Seattle, WA) inserted into the aluminum thermal case. The heater cartridges were controlled by a pair of CN7823 DIN temperature controllers from Omega (Stamford, CT). The temperature controllers measured the temperature of the thermal case using a pair of RTD-850 resistive temperature devices (RTDs, also from Omega) embedded in the thermal case. The temperature controllers had an output accuracy of ± 0.1 °C and the RTDs had a measurement accuracy of ± 0.15 °C. The thermal case was insulated by a custom-built insulation sleeve from LCS Isotherm (Frankfurt, Germany).

Preheating the drift gas above the desired temperature before it entered the showerhead reduced the temperature gradient within the drift tube. This compensated for the heat sink behind the IMS instrument created by the *tof*MS. The drift gas was preheated using a heater built in-house at WSU, consisting of an eight inch length of 1/8 inch stainless steel tubing wrapped with three feet of 90 Ω/ft resistance wire (California Fine Wire Company, Grover Beach, CA) and covered in a protective outer sheath. A Variac supplied a constant voltage to the heater through an electrical plug connected to the resistance wire.

The temperature value of the drift gas used in reduced mobility calculations was measured by two T100-250 probes with an accuracy of ± 0.01 °C coupled to an F200 precision thermometer; both were from Isotech (Colchester, VT). Each probe was inserted into the drift space through the two hollow electrode posts in front of each BN ion gate. Temperature gradients were measured for 24 hours at each setting and the averages between the two measurement points were used in $K_0$ value calculations for each temperature setting. All average temperatures used had a gradient between measurement points of less than 0.1 ºC associated with them.

*1.5 Pressure*

Ambient pressure experiments (approximately 697 Torr for Pullman, WA) used a 230-7420 mercury barometer from NovaLynx (Grass Valley, CA). The barometer had an accuracy of ± 0.2 Torr after correcting for temperature and latitude at the measurement site. Sub-ambient pressures could be achieved using a 640A pressure controller from MKS Instruments (Andover, MA) in conjunction with a DS 42 rotary vane vacuum pump from Agilent Technologies Vacuum Products Division (Lexington, MA). The pressure controller contained a capacitance manometer and had an accuracy of ± 0.5%. The counter current drift gas was maintained at 1.00 ± 0.01 L/min with an 1179A digital mass flow controller and 247D four channel power supply and display, also from MKS instruments. All $K_0$ values reported here were measured at ambient pressure.

## 2. Construction and Operation of the Accurate IMS Drift Tube

*2.1 Drift Rings*

The drift rings that made up the IMS drift tube served to establish the voltage gradient and electric field by which the ions followed towards the detector. The drift rings consisted of ceramic insulator rings and metal electrode rings. The insulator rings were made out of alumina (99.8%, $Al_2O_3$) with an i.d. of 60.5 mm, an o.d. of 69 mm, and a width of 7 mm. The electrode rings were machined from Alloy 46 (National Electronic Alloys, Oakland, NJ); a nickel-iron Alloy (46% Ni). Alloy 46 was used because its coefficient of thermal expansion (7.5 ppm/°C) closely matched that of alumina (7.4 ppm/°C). The electrode rings, shown in the dimetric computer assisted design (CAD) drawing of **Figure 1a**, had an i.d. of 58.4 mm, an o.d. of 66.7 mm, and a width of 8 mm. The electrode rings were machined to feature a small stepped face on each of their front and back faces; shown in the cross-sectional drawings of **Figure 1b** and in detail in **Figure 1c**. The stepped

face was created by a 0.5 mm wide by 0.9 mm high ridge extruding from either side of a 2 mm wide central rim. From either side of this 0.5 mm ridge the electrode portion of the part extended another 2.5 mm. This stepped face served to maintain a face-to-face contact between adjacent rings while creating a cavity into which ceramic adhesive would be injected in a later step. By injecting ceramic adhesive in this manner the known length of the drift tube was not altered by an unknown thickness of adhesive between rings, and the rings remained parallel so as to maintain the homogeneity of the electric field. A 1.45 mm diameter by 10 cm long threaded rod was screwed into a hole at the top of each electrode ring's central rim and served as an electrode post and connection to the voltage divider via pin connectors (Positronic Industries Inc., Springfield, MO).

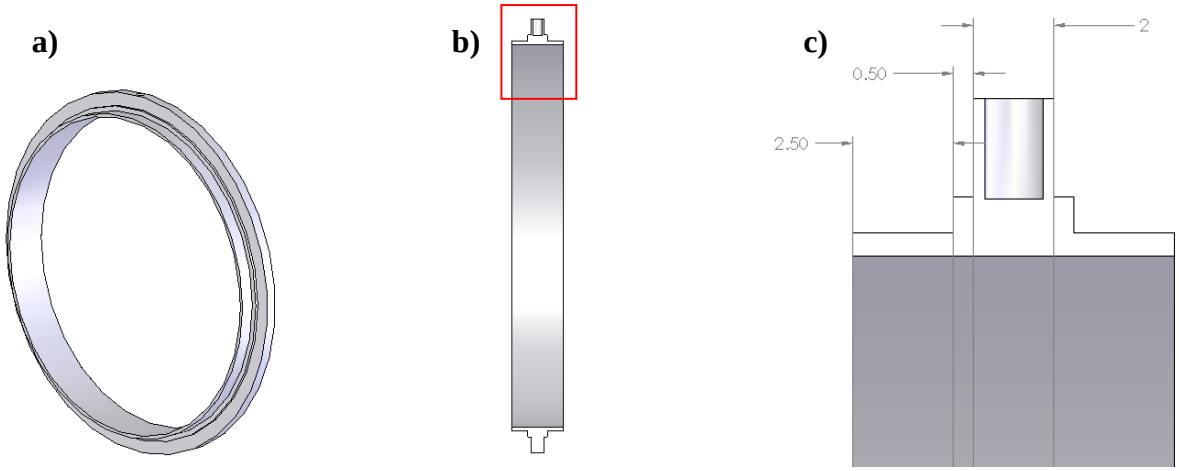


**Figure 1.** CAD drawings of an **a)** Alloy 46 electrode ring; **b)** cross section of the Alloy 46 electrode ring; and **c)** detailed view of the stepped face cross section highlighted by the red box in Figure 1b. Dimensions are in mm.

When the ring portions of the electrodes were fitted within the i.d. of the insulator rings, the faces of the insulator rings made contact with the faces of the 0.5 mm ridge on the electrode rings. This is shown in **Figure 2a** with three electrodes and three insulator rings. This left a 0.5 mm wide cavity between the insulator ring and the face of the central rim on the electrode, as well as a distance of 3 mm between insulator rings, as shown in detail in **Figure 2b**. One electrode ring

in both the reaction and drift regions of the IMS instrument was specially machined to feature a hollow electrode post for the insertion of T100-250 temperature probes to enable the direct measurement of the drift gas temperature. A 1/8 inch Swagelok fitting (Solon, OH) was also attached to the top of these hollow electrode posts to enable the pressure sealing of these ports.

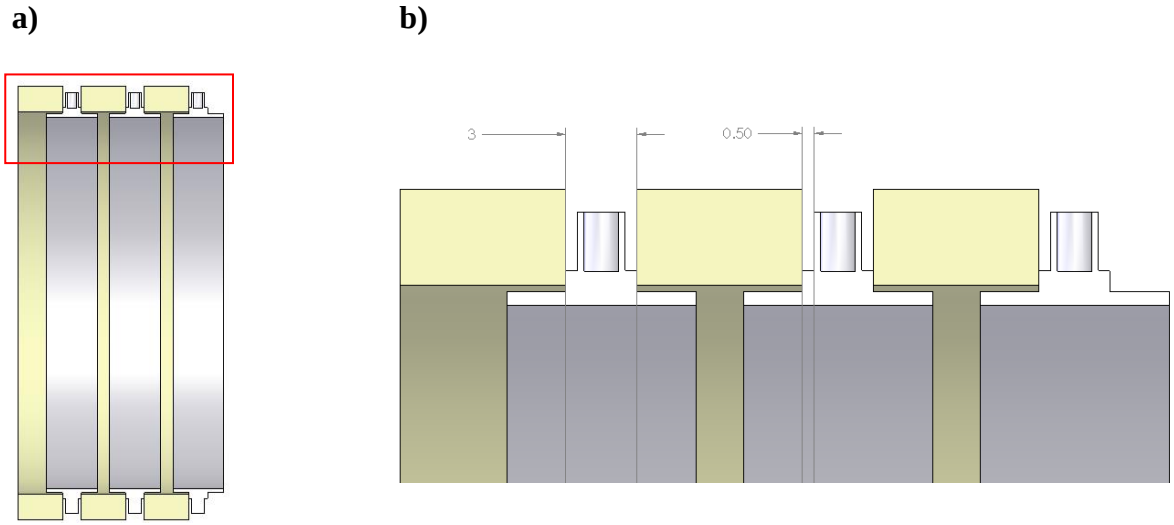


**Figure 2.** CAD drawings of **a)** cross-sectioned view of a stacked ring assembly consisting of three Alloy 46 electrodes (gray) and three ceramic insulator rings (tan); and **b)** detailed view of the spacing of the drift rings highlighted by the red box in Figure 1a.

*2.2 Bradbury-Nielson Ion Gates*

The IMS drift tube contained two BN ion gates, which were used to initiate the drift time measurements, and were constructed using existing methods within this laboratory. Each BN ion gate consisted of a single ceramic insulator ring cut in half radially. A 1.27 mm wide channel was ground into the outer face of each half ring. One side of the channel was also ground down to have an o.d. of 66.18 mm. The smaller o.d. faces of the two BN ion gate halves were then cemented together with an array of parallel 0.003 inch o.d. Alloy 46 wires (California Fine Wire Company, Grover Beach, CA) between them spaced on 0.005 inch centers. Alternating wires were electrically connected to create two interleaved sets of parallel and electrically isolated wires.

*2.3 Ni-63 Ionization Source*

Ni-63 was used to ionize the sample. The ion source was constructed to maintain a hermetic seal and confine the equipotential lines of the drift field to the interior of the drift tube. The Ni-63 ionization source base and interface are shown in **Figure 3a**. The ion source base was made of Alloy 46 and had four ceramic rods mounted to it while a wire mesh screen and cup holding a Ni-63 foil was mounted to the other end of the rods using small stubs attached to the base and Ni-63 cup. This ion source base screwed into the ionization source interface and compressed an alloy 718 c-seal from Jetseal (Spokane, WA) for vacuum sealing. The ionization source interface sat against the front face and inside of a piece of 43.5 mm long alumina tubing with the same o.d. and i.d. as the alumina insulator rings. On the other side of this alumina piece was the first electrode ring of the IMS instrument, with a wire mesh screen spot welded to its front. The wire mesh screen served to shield the equipotential lines within the drift tube from the grounded base plate of the ionization source. This set up straight and vertical equipotential lines to keep the ions on a straight path towards the detector. Both the ion source base and the first electrode were machined to create a 0.5 mm cavity, identical to the ones described in **Figure 2b**, between them and the long alumina piece. When the ion source base was screwed into the ion source interface, as shown in **Figure 3b**, the ceramic rods on the base pushed the screen attached to the Ni-63 containing cup against the screen of the first electrode. This created electrical contact and supplied high voltage to the Ni-63 foil to induce ionization.

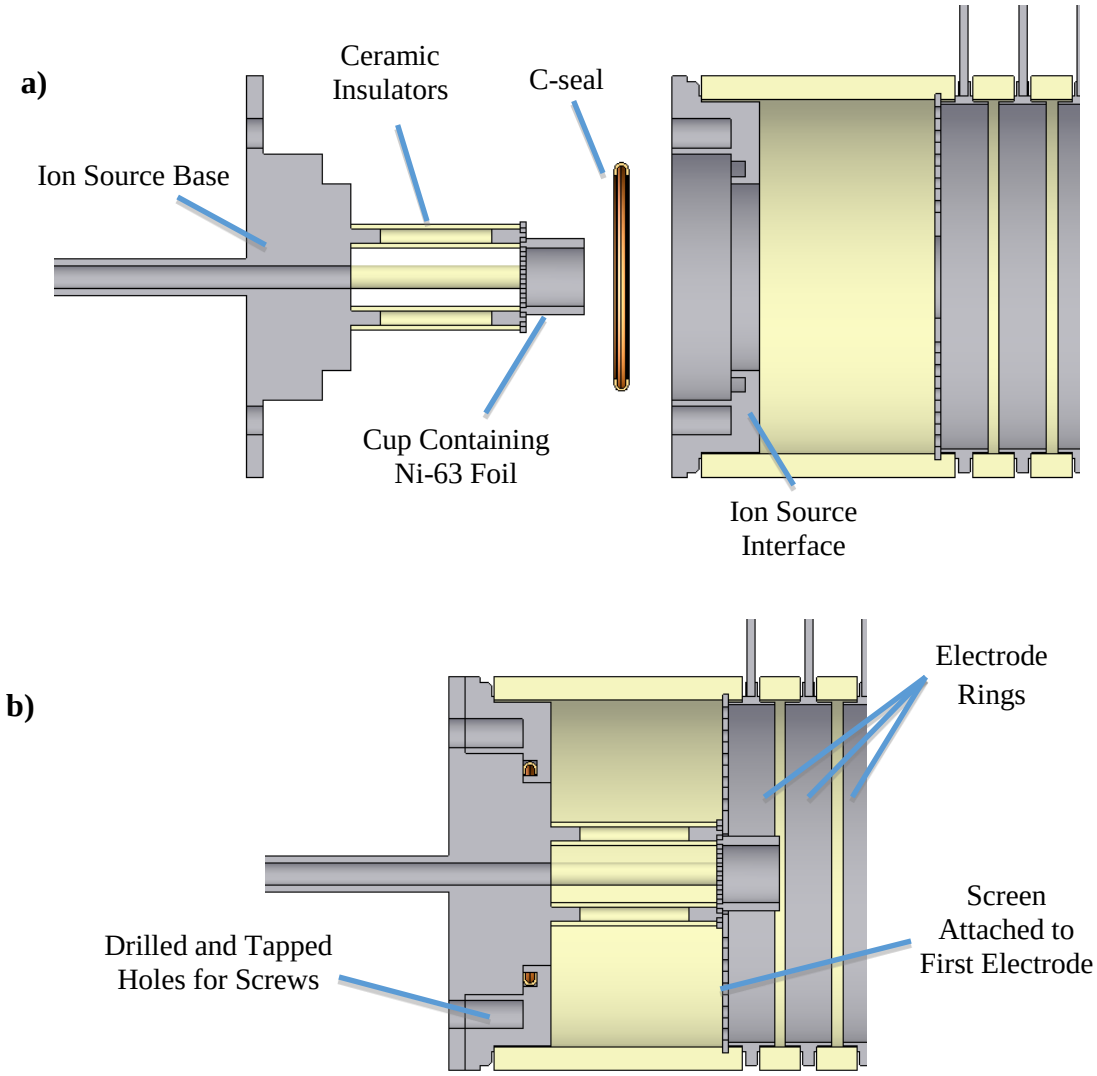


**Figure 3.** CAD drawing of the ionization source base, c-seal, and interface **a)** separated and **b)** joined together to make electrical contact between the Ni-63 cup and first electrode screen as well as compressing the c-seal between the ionization source base and interface.

*2.4 Drift Gas Showerhead*

The last electrode before the *tof*MS vacuum interface served to introduce the neutral counter current flow of drift gas and also contained a Faraday plate for optional standalone analyses without the *tof*MS as the detector. The drift gas was introduced using a "showerhead" design. The drift gas showerhead/Faraday plate assembly, shown in **Figure 4**, was placed behind

the second gate and just before the pressure interface of the *tof*MS. It consisted of a central annular Faraday plate cemented within a piece of insulating alumina tubing using Resbond 920 fast curing ceramic adhesive from Cotronics (Brooklyn, NY). The alumina tubing holding the Faraday plate was likewise cemented within the i.d. of the drift gas entry showerhead. On top of the showerhead were seated three different leads; the first being a metal to ceramic brazed isolator on the left from Solid Sealing Technology, Inc. (Watervliet, NY). This isolator was hollow and served to allow for the attachment of a drift gas line using 1/8 inch Swagelok fittings while keeping the line electrically isolated from the voltage applied to the showerhead. The next two leads were on the right and were in line with one another along the axis of the drift tube. The lead in front was a BNC cable attached to a 1kV feedthrough also from Solid Sealing Technology, Inc. The other end of the feedthrough was spot welded to the backside of the Faraday plate to complete the circuit for standalone Faraday plate analyses. The last lead behind the BNC cable lead was the threaded rod screwed into the showerhead to supply voltage to it. The overall o.d. of the showerhead was the same as the ceramic insulator rings, and its front face was machined to create a 0.5 mm cavity identical to the ones described in **Figure 2b** when placed against the second gate.

**Figure 4.** Front view of the drift gas showerhead assembly showing the Faraday plate and insulating ceramic cemented in the center, and the drift gas isolator (left) and BNC signal lead (right) on top of the showerhead base. The electrode post screwed into and supplying voltage to the base is in line behind the BNC signal lead.

*2.5 Pressure Sealing Procedure*

*a. Drift Ring Joints*

In order to pressure seal each of the joints between the electrode and insulator rings, the two sections of the drift tube with continuous i.d.'s (the drift region and reaction region, excluding the BN ion gates) were mounted separately onto an adjustable mandrel that was then tightly clamped down onto the mounted stack. The mandrel served to keep all drift rings in place during construction and ensure that the electrode rings were concentric and parallel in order to maintain a homogenous electric field. Resbond 920 fast curing ceramic adhesive was injected into the 0.5 mm cavities created by the machined ridges previously described. After allowing to air dry for twenty-four hours, each region was taken off the mandrel and heat cured in an oven at 150 ºC for

an additional twenty-four hours. A light layer of Durapot 801 ceramic potting material, also from Cotronics, was then applied to the cured cement in order to help strengthen the joints. Similarly, the layer of Durapot 801 was allowed to air dry and was then heat cured. After heat curing the Durapot 801, a layer of Celvaseal liquid vacuum leak sealant from Myers Vacuum (Kittanning, PA) was brushed onto the joints and allowed to air dry for two weeks.

After drying, each part was again placed in the oven in order to melt away excess Celvaseal and cure what had permeated into the micropores of the ceramic. The parts were then cleaned of excess Celvaseal using dichloromethane and cotton tipped applicators. This left a layer of Celvaseal cured within the micropores of the drift tube joints. A second layer of Durapot 801 was then applied to the dried layer of Celvaseal in order to encase the vacuum seal layer. Special care was taken to ensure that the second layer of Durapot 801 did not extend past the o.d. of the ceramic insulator rings. Parts that were unable to be mounted on the mandrel (the BN ion gates, showerhead, first electrode, and ionization source interface) were lined up within the rest of the assembly on the bench top and a 36 inch bar clamp was used to fasten the stack to the bench top. This ensured a tight mating of all faces and prevented the rings from separating while injecting the ceramic cement into the remaining joints. The same sealing procedure was then repeated for the remaining joints. The pressure seal was periodically tested during the construction process using a vacuum stage attached to a large rotary vane pump and an analog pressure gauge until the desired pressure was achieved.

*b. Front and Back End of the Drift Tube*

The front end of the drift tube was sealed by the 39.7 mm o.d. by 34.5 mm i.d. c-Seal seen in **Figure 3**. The c-Seal was compressed by screwing down the ion source front plate using eight

socket cap screws. Four springs from McMaster-Carr (Robbinsville, NJ), each with a force of 19 lbs/ft, were mounted equidistantly around four of the screws on the ion source front plate and compressed between the ion source front plate and the front plate of the thermal case holding the IMS instrument assembly. These springs pushed the IMS instrument up against the front of the *tof*MS and compressed a 2.25 inch i.d. x-profile double sealing o-ring (McMaster-Carr) that was placed around a seating ridge on the back of the drift gas showerhead. This double sealing o-ring created a pressure seal between the back of the showerhead and the front of the *tof*MS vacuum interface. The entire assembly is depicted by the dimetric cross-sectional CAD drawing in **Figure 5**. The IMS instrument is shown housed within an insulating ceramic tube, which was in turn housed within the aluminum thermal case built in-house at WSU. The thermal case was attached to the *tof*MS vacuum interface using screws and thumb nuts.

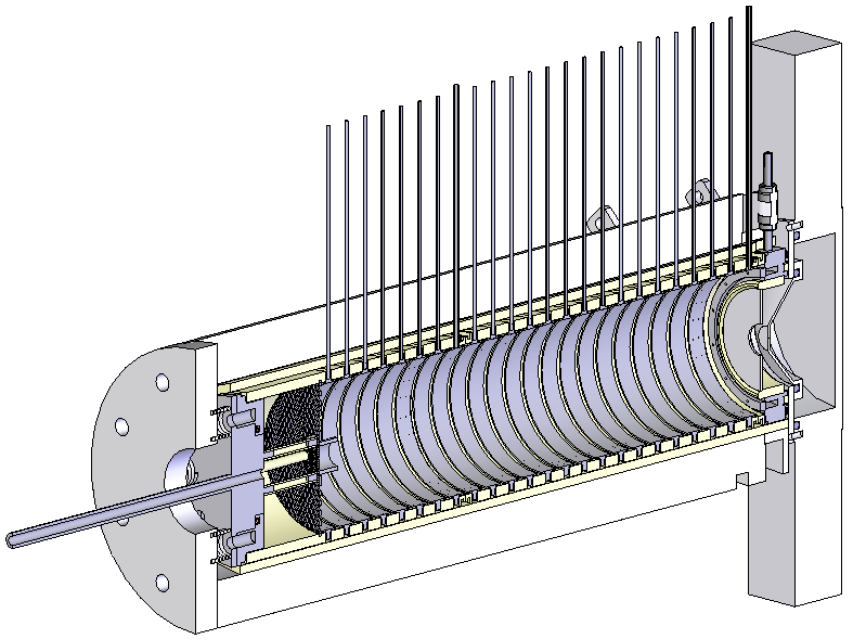

**Figure 5.** Dimetric cross-section CAD drawing of constructed ion mobility spectrometer. Two hollow electrode posts before each gate allow for the insertion of temperature probes to directly measure the temperature of the drift gas as well as the introduction of sample through the first hollow electrode post.

*c. Temperature Probe and Sample Entry Ports*

The specialized electrode rings that allowed for the insertion of the temperature probes and sample also needed to be pressure sealed while still being able to easily connect to the pin connectors of the resistor chain. This was done by modifying two fittings, a 1/8 inch Swagelok cap and an EZRU21 external/internal reducing union from Valco Instruments Inc. Co. (Houston, TX) as shown in **Figure 6**. A small hole was drilled and tapped into each fitting, without going through to the i.d., and a small piece of a threaded rod was screwed into the hole onto which a male pin connector was soldered. The Valco external/internal reducing union was used on the electrode in the reaction region in order to allow for sample introduction into the drift tube via a silica capillary held by an FS1.36 fused silica adapter, also from Valco Instruments. The 1/8 inch Swagelok cap was used on the electrode ring in the drift region.

**Figure 6.** Modified Valco external/internal reducing union (left) and Swagelok cap (right) used to make vacuum tight seals and provide easy electrical contact of the temperature probe drift rings to the resistor chain via the gold pin connectors soldered to the short posts drilled into the parts.

*2.6 Ambient and Reduced Pressure Operation*

Ambient pressure measurements were made by a mercury barometer and the drift gas outlet was left open to the laboratory atmosphere. Sub ambient pressures could be achieved by

connecting the drift gas outlet to the 640A pressure controller and DS 42 rotary vane vacuum pump. The vacuum pump was turned on and an orifice within the pressure controller restricted the flow of gas evacuating from the drift tube to establish the pressure set on the 247D power supply and read out.

*2.7 Sample Introduction*

Headspace vapor samples of volatile compounds were introduced into the instrument by placing 0.5 $\mu$L of neat sample in a 1/8 inch Swagelok cap and attaching the cap to the bottom of an 8 inch length of stainless steel tubing. The sample tee was connected via Swagelok fittings to a compressed air gas tank on one side and to a 250 $\mu$m i.d. by 360 $\mu$m o.d. fused silica capillary via the previously mentioned Valco fittings on the other. The capillary was inserted through the specialized temperature probe port and terminated in the reaction region in the center of the drift tube diameter. The capillary was held in place in the temperature probe port by the previously mentioned Valco fitting adapted for electrical continuity. The orthogonal flow of gas carried the headspace vapors rising from the sample tee through the silica capillary and into the reaction region of the accurate IMS instrument. A 15 kV ceramic isolator from Solid Sealing Technology, Inc ensured electrical isolation of the drift tube from the sample tee. Dimethyl methylphosphonate (DMMP) was the only volatile compound introduced in this manner for this study and was obtained as a 97% pure standard from Sigma Aldrich Chemical Co. (St. Louis, MO).

Nonvolatile compounds were introduced into the instrument by drawing an aliquot of the compound solution into a 17 cm silica capillary (150 $\mu$m i.d., 360 $\mu$m o.d) using a 250 $\mu$L Gastight #1725 syringe and Valco fittings. The solvent was allowed to evaporate for one hour, leaving solid explosives residue inside the capillary. The capillary was then attached to the sample line using

external/internal reducing unions from Valco Instruments Inc. Co. The sample compressed air tank was then operated at 20 psi to carry the dichloromethane vapor (chloride dopant) and explosive sample vapor into the reaction region of the IMS instrument. When the temperature of the drift tube alone was not enough to volatilize the sample from inside the capillary, a secondary heat source was used. A 13.5 cm length of 1/16" o.d. alumina ceramic tubing from McMaster-Carr (Los Angeles, CA) was inserted into the temperature probe/sample introduction port in the reaction region of the instrument so that 0.5 cm of tubing extended into the reaction region of the instrument and 2 cm of tubing extended out of the other end of the sample introduction port. This concealed 11 cm of the tubing within the i.d. of the sample port tubing. An alumina fish spine bead was cemented to the o.d. of the alumina tubing to prevent it from being pushed too far into the instrument. A 50 cm length of 90 Ω/ft resistance wire from Pelican Wire Company Inc. (Naples, FL) was then folded in half, being careful not to damage the insulation, heat treated, and then inserted into the alumina tubing. The resistance wire was heat treated by connecting it to a Variac on the lab bench and slowing turning up the voltage in order to condition the wire to heat. The tip of the resistance wire was inserted 11 cm into the alumina tubing so as to terminate 0.5 cm from the end of the tubing. The alumina (ceramic) tubing served to insulate the resistance wire from the high voltage of the drift tube. The ends of the resistance wire were then attached to a Variac. The sample capillary was inserted down the alumina tubing, and explosives were volatilized from the capillary wall by operating the Variac at 25% full power to heat the resistance wire and capillary. The explosives 2,4,6-trinitrotoluene (TNT), 1,3,5-Trinitroperhydro-1,3,5-triazine (RDX), and pentaerythritol tetranitrate (PETN) were introduced in this manner for this study. All explosives were obtained as 5 mg/mL in methanol, 10 mg/mL in 1:1 methanol:acetonitrile, and 10 mg/mL in acetone, respectively, stock solutions from AccuStandard (New Haven, CT). All stock solutions

were further diluted using HPLC grade methanol from Fisher Scientific (Waltham, MA) to create 0.1 mg/mL, 1 mg/mL, and 1 mg/mL solutions of TNT, RDX, and PETN, respectively.

*2.8 Water Introduction*

A 60 cm silica capillary (5 $\mu$m i.d., 150 $\mu$m o.d.) from Polymicro Technologies was inserted into the drift gas line before the mass flow controller and connected on the other end to a 250 $\mu$L Gastight #1725 syringe from Hamilton (Reno, NV) via Valco fittings. A Fusion 200 syringe pump from Chemyx (Stafford, TX) was operated at 0-85 $\mu$L/hr (± < 1%) at 20 $\mu$L/hr intervals starting after 25 $\mu$L/hr. An increase of 20 $\mu$L/hr in the flow rate of the syringe pump resulted in approximately a 150-170 $ppm_v$ increase in the drift gas water content. After the water introduction junction, a Moisture Image Series 1 hygrometer and probe from GE Measurement and Control (Fairfield, CT) reported the water content of the drift gas. A LabVIEW program written in-house at Washington State University (WSU) recorded the values from the hygrometer every 10 seconds during the acquisition of each IM-*tof*MS spectrum. Other diameter capillaries and syringe pump flow rates may be used to achieve desired drift gas water content levels. HPLC grade water was obtained from Fisher Scientific.

*2.9 Dopant Introduction*

*a. Positive Mode - Ammonia*

A nominal concentration of 10 ppm ammonia was achieved using two permeation tubes (5.3 cm long, 0.64 cm diameter each) that provided a combined permeation rate of 7065.04 ng/min under a flow of air at 1.000 ± 0.002 L/min and 23.4 ºC. The permeation tubes were inserted in-line with the drift gas after the water introduction and before the hygrometer to verify that the ammonia

solution did not increase the measured drift gas water content. The ammonia dopant was present in both the drift region and the reaction region of the IMS instrument. The calculated ammonia concentration at the nominal level of 10 ppm was 10.2 ppm at 23.4°C. The positive mode reactant ions changed from a series of hydronium water clusters to solely ammonium reactant ions in a series of water clusters. Ammonia was present in the drift gas in both the positive and negative ion modes in order to simulate field instrument conditions.

*b. Negative Mode - dichloromethane*

Dichloromethane (chloride) dopant was introduced into the IMS instrument simultaneously with the sample using a silica capillary (5 $\mu$m i.d., 150 $\mu$m o.d.) from Polymicro Technologies that was inserted into the sample line upstream of the capillary containing the sample. The dichloromethane supply capillary was connected to a 250 $\mu$L Gastight #1725 syringe via Valco fittings. A Harvard Apparatus (Holliston, MA) Pump 11 syringe pump was operated at 0.06 $\mu$L/min (±0.01%) to introduce dichloromethane and shift the reactant ion chemistry to produce chloride as the dominant reactant ion. Chloride was present only in the negative ion mode and was only introduced with the sample (as opposed to with the drift gas) in order to simulate field instrument conditions. HPLC grade dichloromethane was obtained from Fisher Scientific.

**3. Assessment of Accuracy**

Previously, Crawford et al. performed an error analysis on a stacked ring IMS-*tof*MS instrument with similar components to this instrument, reporting an accuracy of ± 0.5%.[14] Improvements made when designing the current instrument, as well as the procedures for the

accurate and precise measurement[11] of the five variables in Equation (1), improved the accuracy of $K_0$ value measurements to below ± 0.2%, as shown in **Table 1**.

**Table 1.** Error associated with each variable when calculating $K_0$ values and the source of each error, at 50.21 ± 0.04 ºC and 280 V/cm, on the current accurate IMS instrument.

| Variable (units) | Error | Source of Largest Error |
|---|---|---|
| $L$ (cm) | $S_L = \frac{0.007\ \text{cm}}{16.252\ \text{cm}} = 4 \times 10^{-4}$ | Calipers |
| $V$ (V) | $S_V = \frac{0.2\ \text{V}}{4533.1\ \text{V}} = 4 \times 10^{-5}$ | High Voltage Divider Probe and Digital Multimeter |
| $t_d$ (s) | $S_{t_d} = \frac{1 \times 10^{-9}\ \text{s}}{1 \times 10^{-2}\ \text{s}} = 1 \times 10^{-7}$ | *tof*MS clock rate |
| $T$ (K) | $S_T = \frac{0.04\ \text{K}}{323.36\ \text{K}} = 1 \times 10^{-4}$ | Drift Gas Temperature Gradient |
| $P$ (Torr) | $S_P = \frac{0.2\ \text{Torr}}{690\ \text{Torr}} = 3 \times 10^{-4}$ | Mercury Barometer |

Propagating the error associated with each variable in **Table 1** through Equation (1) produces an error of ± 0.001 $cm^2V^{-1}s^{-1}$ for a $K_0$ value of 1 and ± 0.002 $cm^2V^{-1}s^{-1}$ for a $K_0$ value of 2, amounting to an optimized error ± 0.1% for obtained $K_0$ values. Improvements to the instrument design and procedures contributed to this improved error. The current accurate IMS instrument used the same measurement and control equipment for the five variables as the drift tube built by Crawford et al., except for the high voltage power supplies, temperature controller, and the mass flow and pressure controllers. The high voltage power supplies first used had a 15 ppm output ripple, while the output ripple of the current high voltage power supply was 1 ppm. This reduced the variability of the applied electric field strength. Design elements of the accurate IMS instrument also improved the accuracy. The electrodes within the stacked ring drift tube built by Crawford et al. were not fixed in place but were stacked and held together under spring tension. The current accurate IMS instrument's electrodes and ceramic insulator rings were fixed in place

and assembled to be concentric and parallel. This eliminated inhomogeneity within the electric field created by inconsistent stacking. The drift tube built by Crawford et al. only contained one BN ion gate and the residence time within the *tof*MS was determined by plotting the drift time of the ion as a function of the inverse voltage drop, which has been shown to be a more inaccurate method.[12] Using two BN ion gates in the current accurate IMS instrument directly correlated the measured length to the measured drift time. Crawford et al. were also only able to reduce the drift gas temperature gradients between the BN ion gate and the *tof*MS vacuum interface inlet to within ± 0.5 ºC. The method for pre-heating the drift gas in the current drift tube in which a resistive wire heater was used instead improved the drift gas temperature gradients between BN ion gates by an order of magnitude to a maximum of ± 0.05 ºC.[11] The pressure measurement taken from the mercury barometer was also corrected for temperature and gravity due to latitude, which was not done in the past.

**4. Assessment of Hermetic Seal**

Before the final assembly step, in which the separate drift tube sections were cemented together, the BN ion gates, the drift region, and the reaction region were separately tested for their ability to maintain an internal vacuum. Each BN ion gate was able to achieve an internal pressure of 0.01 Torr and the drift region and reaction region were each able to achieve an internal pressure of 0.02 Torr. Upon completion of the drift tube construction and installation onto the *tof*MS, the DS42 vacuum pump was attached to the drift gas outlet but left in the off position and with no drift gas flowing. It was observed that the pinhole of the *tof*MS alone was able to evacuate the drift tube to 69 torr. The pressures within the two-stage vacuum interface also decreased from 1.7 and $3.5\times10^{-2}$ Torr to $3.0\times10^{-1}$ and $9.9\times10^{-3}$ Torr, respectively. When the vacuum pump was turned on

while still keeping the drift gas flow off, the pressure within the drift tube further decreased to 10 Torr and the *tof*MS interface pressures decreased to $8.0\times10^{-2}$ and $6.4\times10^{-3}$ Torr. Such a vacuum is more than sufficient to obtain desired pressures down to 0.5 atmospheres in order to conduct pressure experiments as well as ensure the safe execution of experiments involving hazardous chemicals such as chemical warfare agents. The ability to conduct these sub ambient experiments was further demonstrated when the mass flow and pressure controllers were able to achieve a drift gas flow rate measurement of 1 L/min and an internal pressure of 200 Torr, respectively.

The performance of the instrument was tested under reduced pressures by collecting spectra of DMMP at 202 Torr. **Figure 7** shows the reduced pressure spectrum compared to a spectrum taken at an ambient pressure of approximately 697 Torr. Both pressure conditions produced the same reactant and product ions, as shown in the *x*-axis of **Figure 7**. The three drift time peaks corresponded to the proton-bound dimer of ammonia [$(NH_3)_2H^+$, *m/z* 35], the ammoniated monomer of DMMP [$DMMP(NH_4)^+$, *m/z* 142], and the ammonium-bound dimer of DMMP [$(DMMP)_2(NH_4)^+$, *m/z* 266]. Each of these ions also fragmented in the *tof*MS vacuum interface into ammonium [$NH_4^+$, *m/z* 18], the protonated monomer of DMMP [$DMMPH^+$, *m/z* 125], and the proton-bound dimer of DMMP [$(DMMP)_2H^+$, *m/z* 249]. All three drift time peaks shifted to faster drift times and became sharper at 202 Torr. The resolving power of the three peaks also decreased as they shifted closer to one another. This demonstrates that the accurate IMS instrument can be hermetically sealed and is operational at reduced pressures and will allow for the analysis of hazardous chemicals such as active CWA.

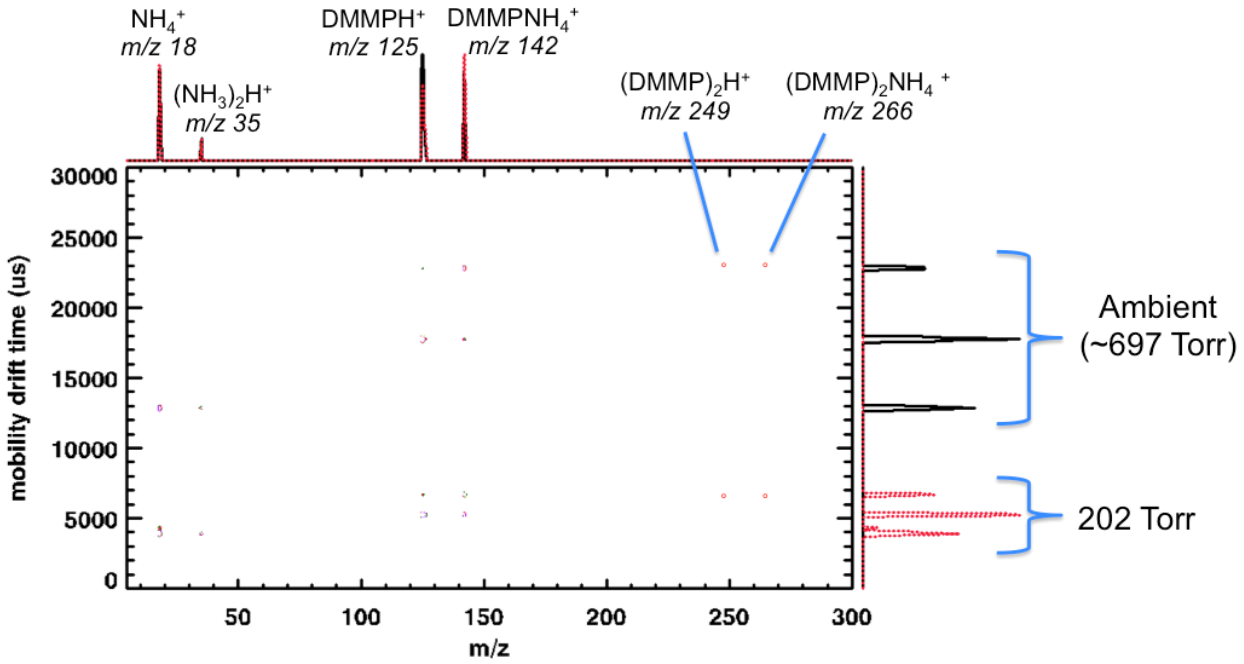


**Figure 7.** Overlay of spectra of DMMP at ambient pressure (black trace) and reduced pressure (red trace). Both spectra were taken at 425 V/cm and the drift gas had a moisture content of < 5 $ppm_v$. As the pressure inside the IMS instrument was decreased, the drift time peaks shifted to faster drift times, higher resolution, and lower resolving power.

## 5. Initial Database of Accurate $K_0$ Values for Compounds of Interest Analyzed

The accurate $K_0$ values of the compounds of interest studied (ammonia reactant ion, DMMP, TNT, Tetryl, and PETN) are shown in **Table 2** through **Table 9**. Compounds were analyzed as a function of temperature, drift gas water content, and electric field. Compounds were analyzed as a function of temperature and drift gas water content because it has been shown that $K_0$ values may change due to varying degrees of clustering reactions occurring within the drift tube. The response to these two variables was also investigated in order to potentially develop DMMP as an accurate mobility reference standard and empirically measure the drift gas water content using the ratio of monomer to dimer $K_0$ values.[10] Compounds were analyzed as a function of electric field because of a newly discovered phenomenon discovered by Hauck et al. showing a dependence of the $K_0$ value on low electric fields.[11,12]

**Table 2.** Reduced mobility values of the proton bound dimer of ammonia, the ammoniated monomer of DMMP, and the ammonium bound dimer of DMMP as a function of drift gas water content at four drift gas temperatures and with the electric field strength held constant at 280.2 V/cm. The precision followed by the accuracy of each data point is reported in parenthesis.

| **Average Drift Gas Temperature** *°C* | **Average Drift Gas Water Content** *$ppm_v H_2O$* | $K_0$ value (precision, accuracy) *$cm^2V^{-1}s^{-1}$* | | |
|---|---|---|---|---|
| | | $NH_3(NH_4)^+$ *m/z 35* | $DMMP(NH_4)^+$ *m/z 142* | $(DMMP)_2(NH_4)^+$ *m/z 266* |
| | 1.33 ± 0.01 | 2.328 (± 0.002, ± 0.002) | 1.671 (± 0.001, ± 0.002) | 1.323 (± 0.002, ± 0.002) |
| | 166 ± 5 | 2.185 (± 0.003, ± 0.003) | 1.645 (± 0.002, ± 0.002) | 1.319 (± 0.001, ± 0.001) |
| 26.18 ± 0.03 | 352 ± 5 | 2.125 (± 0.001, ± 0.002) | 1.6280 (± 0.0004, ± 0.002) | 1.317 (± 0.001, ± 0.001) |
| | 509 ± 1 | 2.079 (± 0.001, ± 0.002) | 1.615 (± 0.001, ± 0.002) | 1.3132 (± 0.0005, ± 0.001) |
| | 641 ± 3 | 2.056 (± 0.001, ± 0.002) | 1.608 (± 0.002, ± 0.002) | 1.312 (± 0.002, ± 0.002) |
| | 1.632 ± 0.002 | 2.347 (± 0.001, ± 0.002) | 1.676 (± 0.001, ± 0.002) | 1.323 (± 0.002, ± 0.002) |
| | 130 ± 16 | 2.217 (± 0.002, ± 0.002) | 1.654 (± 0.001, ± 0.002) | 1.320 (± 0.001, ± 0.001) |
| 30.05 ± 0.01 | 257 ± 2 | 2.161 (± 0.002, ± 0.002) | 1.640 (± 0.001, ± 0.002) | 1.319 (± 0.001, ± 0.001) |
| | 421 ± 2 | 2.111 (± 0.001, ± 0.002) | 1.628 (± 0.001, ± 0.002) | 1.316 (± 0.001, ± 0.001) |
| | 580 ± 3 | 2.079 (± 0.001, ± 0.002) | 1.617 (± 0.001, ± 0.002) | 1.312 (± 0.001, ± 0.001) |
| | 1.036 ± 0.007 | 2.386 (± 0.002, ± 0.002) | 1.6926 (± 0.0003, ± 0.002) | 1.323 (± 0.001, ± 0.001) |
| | 144 ± 4 | 2.263 (± 0.002, ± 0.002) | 1.671 (± 0.002, ± 0.002) | 1.321 (± 0.001, ± 0.001) |
| 40.15 ± 0.01 | 340 ± 4 | 2.199 (± 0.004, ± 0.004) | 1.656 (± 0.001, ± 0.002) | 1.320 (± 0.001, ± 0.001) |
| | 452 ± 14 | 2.167 (± 0.001, ± 0.002) | 1.648 (± 0.002, ± 0.002) | 1.3192 (± 0.0003, ± 0.001) |
| | 606 ± 2 | 2.1322 (± 0.0002, ± 0.002) | 1.640 (± 0.001, ± 0.002) | 1.317 (± 0.001, ± 0.001) |
| | 1.494 ± 0.009 | 2.420 (± 0.001, ± 0.002) | 1.7114 (± 0.0002, ± 0.002) | 1.323 (± 0.001, ± 0.001) |
| | 166 ± 2 | 2.298 (± 0.001, ± 0.002) | 1.6873 (± 0.0003, ± 0.002) | 1.320 (± 0.001, ± 0.001) |
| 50.21 ± 0.04 | 342 ± 1 | 2.244 (± 0.001, ± 0.002) | 1.675 (± 0.001, ± 0.002) | 1.320 (± 0.001, ± 0.001) |
| | 477 ± 1 | 2.2119 (± 0.0003, ± 0.002) | 1.666 (± 0.001, ± 0.002) | 1.319 (± 0.001, ± 0.001) |
| | 621 ± 2 | 2.181 (± 0.001, ± 0.002) | 1.6589 (± 0.0003, ± 0.002) | 1.3176 (± 0.0004, ± 0.001) |

**Table 3.** Reduced ion mobility values of the proton bound dimer of ammonia, the ammoniated monomer of DMMP, and the ammonium bound dimer of DMMP as a function of drift gas water content at four electric field strengths and with the drift gas temperature held constant at 30.05 ± 0.01 °C. The precision followed by the accuracy of each data point is reported in parentheses.

| **Electric Field Strength** *V/cm* | **Average Drift Gas Water Content** *$ppm_v H_2O$* | $K_0$ value (precision, accuracy) *$cm^2V^{-1}s^{-1}$* | | |
|---|---|---|---|---|
| | | $NH_4^+$ *m/z 35* | $DMMP(NH_4)^+$ *m/z 142* | $DMMP_2(NH_4)^+$ *m/z 266* |
| | 1.632 ± 0.002 | 2.347 (± 0.001, ± 0.001) | 1.676 (± 0.001, ± 0.002) | 1.323 (± 0.002, ± 0.002) |
| | 130 ± 16 | 2.217 (± 0.002, ± 0.002) | 1.654 (± 0.001, ± 0.002) | 1.320 (± 0.001, ± 0.001) |
| 280.2 | 257± 2 | 2.161 (± 0.002, ± 0.002) | 1.640 (± 0.001, ± 0.002) | 1.319 (± 0.001, ± 0.001) |
| | 421 ± 2 | 2.111 (± 0.001, ± 0.001) | 1.628 (± 0.001, ± 0.002) | 1.316 (± 0.001, ± 0.001) |
| | 580 ± 3 | 2.079 (± 0.001, ± 0.001) | 1.617 (± 0.001, ± 0.002) | 1.312 (± 0.001, ± 0.001) |
| | 0.899 ± 0.004 | 2.349 (± 0.001, ± 0.002) | 1.6748 (± 0.0004, ± 0.002) | 1.321 (± 0.001, ± 0.001) |
| | 138 ± 13 | 2.209 (± 0.006, ± 0.006) | 1.652 (± 0.001, ± 0.002) | 1.3187 (± 0.0002, ± 0.001) |
| 350.1 | 216 ± 1 | 2.168 (± 0.001, ± 0.002) | 1.640 (± 0.001, ± 0.002) | 1.317 (± 0.001, ± 0.001) |
| | 380 ± 13 | 2.117 (± 0.003, ± 0.003) | 1.627 (± 0.001, ± 0.002) | 1.312 (± 0.001, ± 0.001) |
| | 498 ± 4 | 2.086 (± 0.001, ± 0.002) | 1.619 (± 0.002, ± 0.002) | 1.311 (± 0.001, ± 0.001) |
| | 1.933 ± 0.004 | 2.341 (± 0.001, ± 0.002) | 1.6715 (± 0.0005, ± 0.002) | 1.319 (± 0.001, ± 0.001) |
| | 151 ± 1 | 2.204 (± 0.001, ± 0.002) | 1.647 (± 0.001, ± 0.002) | 1.314 (± 0.001, ± 0.001) |
| 450.7 | 318 ± 2 | 2.146 (± 0.002, ± 0.002) | 1.632 (± 0.001, ± 0.002) | 1.313 (± 0.001, ± 0.001) |
| | 437 ± 1 | 2.107 (± 0.001, ± 0.002) | 1.622 (± 0.001, ± 0.002) | 1.311 (± 0.001, ± 0.001) |
| | 567 ± 2 | 2.076 (± 0.001, ± 0.002) | 1.6131 (± 0.0004, ± 0.002) | 1.308 (± 0.001, ± 0.001) |
| | 1.848 ± 0.002 | 2.339 (± 0.001, ± 0.002) | 1.670 (± 0.001, ± 0.002) | 1.319 (± 0.002, ± 0.002) |
| | 145 ± 2 | 2.208 (± 0.002, ± 0.002) | 1.647 (± 0.001, ± 0.002) | 1.315 (± 0.001, ± 0.001) |
| 525.1 | 324 ± 5 | 2.1423 (± 0.0005, ± 0.002) | 1.631 (± 0.002, ± 0.002) | 1.3134 (± 0.0005, ± 0.001) |
| | 479 ± 1 | 2.090 (± 0.002, ± 0.002) | 1.617 (± 0.001, ± 0.002) | 1.310 (± 0.002, ± 0.002) |
| | 579 ± 1 | 2.071 (± 0.001, ± 0.002) | 1.612 (± 0.001, ± 0.002) | 1.3077 (± 0.0005, ± 0.001) |

**Table 4.** Reduced mobility values of the proton-abstracted ion of TNT as a function of drift gas water content at four drift gas temperatures and with the electric field strength held constant at 280.2 V/cm. The precision followed by the accuracy of each data point is reported in parentheses.

| **Average Drift Gas Temperature** *°C* | **Average Drift Gas Water Content** *$ppm_v\ H_2O$* | ***$K_0$*** value (precision, accuracy) *$cm^2V^{-1}s^{-1}$* |
|---|---|---|
| | | $(TNT\text{-}H)^-$ *m/z 226* |
| 26.18 ± 0.03 | 1.107 ± 0.004 | 1.568 (± 0.002, ± 0.002) |
| | 173 ± 4 | 1.564 (± 0.001, ± 0.002) |
| | 343 ± 1 | 1.564 (± 0.001, ± 0.002) |
| | 507 ± 18 | 1.562 (± 0.001, ± 0.002) |
| | 628 ± 6 | 1.558 (± 0.001, ± 0.002) |
| 30.05 ± 0.01 | 0.887 ± 0.001 | 1.5679 (± 0.0005, ± 0.002) |
| | 164 ± 3 | 1.566 (± 0.001, ± 0.002) |
| | 339 ± 1 | 1.565 (± 0.001, ± 0.002) |
| | 420 ± 12 | 1.563 (± 0.002, ± 0.002) |
| | 630 ± 10 | 1.562 (± 0.001, ± 0.002) |
| 40.15 ± 0.01 | 1.36 ± 0.02 | 1.5700 (± 0.0002, ± 0.002) |
| | 160 ± 2 | 1.569 (± 0.001, ± 0.002) |
| | 325 ± 2 | 1.567 (± 0.001, ± 0.002) |
| | 472 ± 9 | 1.567 (± 0.002, ± 0.002) |
| | 589 ± 12 | 1.5645 (± 0.0004, ± 0.002) |
| 50.21 ± 0.04 | 0.840 ± 0.001 | 1.571 (± 0.002, ± 0.002) |
| | 151 ± 4 | 1.5687 (± 0.0003, ± 0.002) |
| | 312 ± 4 | 1.567 (± 0.002, ± 0.002) |
| | 455 ± 9 | 1.566 (± 0.001, ± 0.002) |
| | 568 ± 6 | 1.566 (± 0.001, ± 0.002) |

**Table 5.** Reduced mobility values of the proton-abstracted ion of TNT as a function of drift gas water content at four electric field strengths and with the drift gas temperature held constant at 30.05 ± 0.01 °C. The precision followed by the accuracy of each data point is reported in parentheses.

| **Electric Field Strength** *V/cm* | **Average Drift Gas Water Content** *$ppm_v$ $H_2O$* | ***$K_0$*** value (precision, accuracy) *$cm^2V^{-1}s^{-1}$* |
|---|---|---|
| | | $(TNT\text{-}H)^-$ *m/z 226* |
| 280.7 | 0.887 ± 0.001 | 1.5679 (± 0.0005, ± 0.002) |
| | 164 ± 3 | 1.566 (± 0.001, ± 0.002) |
| | 339 ± 1 | 1.565 (± 0.001, ± 0.002) |
| | 420 ± 12 | 1.563 (± 0.002, ± 0.002) |
| | 630 ± 10 | 1.562 (± 0.001, ± 0.002) |
| 350.3 | 1.14 ± 0.02 | 1.5637 (± 0.0004, ± 0.002) |
| | 185 ± 20 | 1.562 (± 0.001, ± 0.002) |
| | 350 ± 6 | 1.561 (± 0.002, ± 0.002) |
| | 472 ± 35 | 1.559 (± 0.001, ± 0.002) |
| | 643 ± 31 | 1.560 (± 0.001, ± 0.002) |
| 450.8 | 1.450 ± 0.008 | 1.560 (± 0.001, ± 0.002) |
| | 172 ± 14 | 1.558 (± 0.002, ± 0.002) |
| | 332 ± 1 | 1.556 (± 0.001, ± 0.002) |
| | 455 ± 17 | 1.5567 (± 0.0004, ± 0.002) |
| | 551 ± 4 | 1.556 (± 0.001, ± 0.002) |
| 525.3 | 1.75± 0.01 | 1.560 (± 0.001, ± 0.002) |
| | 176 ± 34 | 1.558 (± 0.001, ± 0.002) |
| | 353 ± 12 | 1.558 (± 0.001, ± 0.002) |
| | 519 ± 5 | 1.555 (± 0.002, ± 0.002) |
| | 601 ± 11 | 1.553 (± 0.001, ± 0.002) |

**Table 6.** Reduced mobility values of the chloride adduct of RDX as a function of drift gas water content at four drift gas temperatures and with the electric field strength held constant at 280.2 V/cm. The precision followed by the accuracy of each data point is reported in parentheses.

| **Average Drift Gas Temperature** | **Average Drift Gas Water Content** | ***K₀*** value (precision, accuracy) |
|---|---|---|
| *°C* | *$ppm_v H_2O$* | *$cm^2V^{-1}s^{-1}$* |
| | | $(RDX+Cl)^-$ *m/z 257* |
| 26.18 ± 0.03 | 1.680 ± 0.005 | 1.506 (± 0.001, ± 0.002) |
| | 172 ± 38 | 1.476 (± 0.001, ± 0.002) |
| | 340 ± 1 | 1.464 (± 0.001, ± 0.002) |
| | 490 ± 8 | 1.452 (± 0.002, ± 0.002) |
| | 601 ± 13 | 1.444 (± 0.001, ± 0.001) |
| 30.05 ± 0.01 | 2.707 ± 0.004 | 1.5059 (± 0.0003, ± 0.002) |
| | 176 ± 51 | 1.476 (± 0.002, ± 0.002) |
| | 342 ± 9 | 1.461 (± 0.001, ± 0.002) |
| | 493 ± 6 | 1.451 (± 0.002, ± 0.002) |
| | 625 ± 9 | 1.444 (± 0.002, ± 0.002) |
| 40.15 ± 0.01 | 1.31 ± 0.07 | 1.509 (± 0.001, ± 0.002) |
| | 157 ± 9 | 1.488 (± 0.002, ± 0.002) |
| | 277 ± 47 | 1.477 (± 0.002, ± 0.002) |
| | 412 ± 1 | 1.470 (± 0.002, ± 0.002) |
| | 589 ± 12 | 1.460 (± 0.002, ± 0.002) |
| 50.21 ± 0.04 | 1.068 ± 0.004 | 1.5086 (± 0.0004, ± 0.002) |
| | 147 ± 4 | 1.495 (± 0.001, ± 0.002) |
| | 233 ± 2 | 1.4894 (± 0.0002, ± 0.002) |
| | 312 ± 4 | 1.4845 (± 0.0002, ± 0.002) |
| | 387 ± 3 | 1.479 (± 0.002, ± 0.002) |
| | 457 ± 1 | 1.479 (± 0.002, ± 0.002) |
| | 574 ± 9 | 1.472 (± 0.001, ± 0.002) |

**Table 7.** Reduced mobility values of the chloride adduct of RDX as a function of drift gas water content at four electric field strengths and with the drift gas temperature held constant at 30.05 ± 0.01 °C. The precision followed by the accuracy of each data point is reported in parentheses.

| **Electric Field Strength** *V/cm* | **Average Drift Gas Water Content** *$ppm_v$ $H_2O$* | ***$K_0$*** value (precision, accuracy) *$cm^2V^{-1}s^{-1}$* |
|---|---|---|
| | | $(RDX+Cl)^-$ *m/z 257* |
| 280.6 | 2.707 ± 0.004 | 1.5059 (± 0.0003, ± 0.002) |
| | 176 ± 51 | 1.476 (± 0.002, ± 0.002) |
| | 342 ± 9 | 1.461 (± 0.001, ± 0.002) |
| | 493 ± 6 | 1.451 (± 0.002, ± 0.002) |
| | 625 ± 9 | 1.444 (± 0.002, ± 0.002) |
| 350.0 | 2.80 ± 0.01 | 1.502 (± 0.001, ± 0.002) |
| | 180 ± 51 | 1.472 (± 0.002, ± 0.002) |
| | 332 ± 3 | 1.460 (± 0.001, ± 0.002) |
| | 461 ± 12 | 1.450 (± 0.002, ± 0.002) |
| | 585 ± 13 | 1.443 (± 0.001, ± 0.001) |
| 450.2 | 1.463 ± 0.003 | 1.499 (± 0.001, ± 0.002) |
| | 171 ± 32 | 1.463 (± 0.002, ± 0.002) |
| | 338 ± 7 | 1.444 (± 0.002, ± 0.001) |
| | 481 ± 8 | 1.440 (± 0.001, ± 0.001) |
| | 643 ± 7 | 1.432 (± 0.002, ± 0.001) |
| 525.0 | 2.983 ± 0.004 | 1.499 (± 0.001, ± 0.002) |
| | 176 ± 46 | 1.468 (± 0.002, ± 0.002) |
| | 340 ± 5 | 1.455 (± 0.001, ± 0.002) |
| | 485 ± 1 | 1.447 (± 0.001, ± 0.002) |
| | 632 ± 16 | 1.437 (± 0.001, ± 0.001) |

**Table 8.** Reduced mobility values of the chloride adduct of PETN as a function of drift gas water content at four drift gas temperatures and with the electric field strength held constant at 280.2 V/cm. The precision followed by the accuracy of each data point is reported in parentheses.

| **Average Drift Gas Temperature** | **Average Drift Gas Water Content** | $K_0$ value (precision, accuracy) |
|---|---|---|
| *°C* | $ppm_v\ H_2O$ | $cm^2V^{-1}s^{-1}$ |
| | | $(PETN+Cl)^-$ |
| | | *m/z 351* |
| 26.18 ± 0.03 | 1.436 ± 0.004 | 1.260 (± 0.001, ± 0.001) |
| | 159 ± 2 | 1.241 (± 0.002, ± 0.002) |
| | 321 ± 4 | 1.235 (± 0.001, ± 0.001) |
| | 444 ± 3 | 1.232 (± 0.001, ± 0.001) |
| | 608 ± 37 | 1.223 (± 0.002, ± 0.002) |
| 30.05 ± 0.01 | 1.754 ± 0.004 | 1.261 (± 0.001, ± 0.001) |
| | 155 ± 3 | 1.240 (± 0.001, ± 0.001) |
| | 317 ± 2 | 1.231 (± 0.002, ± 0.002) |
| | 449 ± 2 | 1.227 (± 0.001, ± 0.001) |
| | 576 ± 14 | 1.2218 (± 0.0005, ± 0.001) |
| 40.15 ± 0.01 | 1.36 ± 0.02 | 1.2611 (± 0.0001, ± 0.001) |
| | 162 ± 1 | 1.249 (± 0.001, ± 0.001) |
| | 323 ± 6 | 1.2406 (± 0.0002, ± 0.001) |
| | 438 ± 20 | 1.236 (± 0.001, ± 0.001) |
| | 542 ± 3 | 1.234 (± 0.002, ± 0.002) |
| 50.208 ± 0.036 | 0.840 ± 0.001 | 1.262 (± 0.001, ± 0.001) |
| | 151 ± 4 | 1.250 (± 0.001, ± 0.001) |
| | 312 ± 4 | 1.2426 (± 0.0002, ± 0.001) |
| | 455 ± 9 | 1.237 (± 0.002, ± 0.002) |
| | 568 ± 6 | 1.233 (± 0.001, ± 0.001) |

**Table 9.** Reduced mobility values of the chloride adduct of PETN as a function of drift gas water content at four electric field strengths and with the drift gas temperature held constant at 30.05 ± 0.01 °C. The precision followed by the accuracy of each data point is reported in parentheses.

| **Electric Field Strength** *V/cm* | **Average Drift Gas Water Content** $ppm_v\ H_2O$ | $K_0$ value (precision, accuracy) $cm^2V^{-1}s^{-1}$ |
|---|---|---|
| | | $(PETN+Cl)^-$ *m/z 351* |
| 280.8 | 1.754 ± 0.004 | 1.261 (± 0.001, ± 0.001) |
| | 155 ± 3 | 1.240 (± 0.001, ± 0.001) |
| | 317 ± 2 | 1.231 (± 0.002, ± 0.002) |
| | 449 ± 2 | 1.227 (± 0.001, ± 0.001) |
| | 576 ± 14 | 1.2218 (± 0.0005, ± 0.001) |
| 350.1 | 2.74 ± 0.03 | 1.258 (± 0.001, ± 0.001) |
| | 171 ± 2 | 1.233 (± 0.001, ± 0.001) |
| | 329 ± 6 | 1.2294 (± 0.0003, ± 0.001) |
| | 462 ± 3 | 1.221 (± 0.001, ± 0.001) |
| | 616 ± 3 | 1.218 (± 0.002, ± 0.002) |
| 450.6 | 1.73 ± 0.03 | 1.258 (± 0.001, ± 0.001) |
| | 166 ± 37 | 1.233 (± 0.001, ± 0.001) |
| | 326 ± 1 | 1.225 (± 0.001, ± 0.001) |
| | 465 ± 38 | 1.218 (± 0.002, ± 0.002) |
| | 602 ± 4 | 1.214 (± 0.001, ± 0.001) |
| 524.9 | 2.75 ± 0.01 | 1.256 (± 0.001, ± 0.001) |
| | 177 ± 57 | 1.236 (± 0.001, ± 0.001) |
| | 333 ± 29 | 1.223 (± 0.001, ± 0.001) |
| | 465 ± 17 | 1.221 (± 0.001, ± 0.001) |
| | 609 ± 32 | 1.216 (± 0.002, ± 0.002) |

## 6. Future Directions and Conclusions

The accurate IMS-*tof*MS instrument detailed in this report has been successfully delivered the Edgewood Chemical Biological Center for permanent installation. Using the data reported here, and any data collected in the future, a database of accurate $K_0$ values will be developed for compounds of interest. The reported $K_0$ values are accurate to ± 0.2% or better. This is more than an order of magnitude improvement upon previously reported accuracies for measurements of $K_0$ values. Work to be done includes the evaluation of potential mobility reference standards to determine the best to use during the calibration process.

The data collected using this instrument will be used to create an improved detection algorithm for IMS-based field instruments. The rate of false positive alarms on IMS-based field instruments will decrease through the use of these accurate $K_0$ values by propagating a lower degree of error when establishing detection windows. The instrument will still be able to maintain a low rate of false negative responses by first using a correction factor in order to shift the mobility scale to the proper position based on the initial uncalibrated response of the instrument and the correct $K_0$ values of ions required to be used. The algorithm will determine the correct $K_0$ values to use for the mobility reference standard and compound of interest using a matrix a values, similar to the ones reported here, that incorporate the operating parameters of the instrument. In this way the IMS-based field instruments will be improved through only software changes and no hardware changes.

## 7. References


1. Eiceman, G. A.; Karpas, Z.; Hill, H. H., Jr. *Ion Mobility Spectrometry*, Third ed.; CRC Press: Boca Raton, FL, 2014.

2. Kanu, A. B.; Haigh, P. E.; Hill, H. H., Jr. *Anal. Chim. Acta* **2005**, *553*, 148-159.

3. Crawford, C. L.; Hauck, B. C.; Tufariello, J. A.; Harden, C. S.; McHugh, V.; Siems, W. F.; Hill, H. H., Jr. *Talanta* **2012**, *101*, 161-170.

4. Fernández-Maestre, R.; Harden, C. S.; Ewing, R. G.; Crawford, C. L.; Hill, H. H., Jr. *Analyst* **2010**, *135*, 1433-1442.

5. Eiceman, G. A.; Nazarov, E. G.; Stone, J. A. *Anal. Chim. Acta* **2003**, *493*, 185-194.

6. Ochoa, M. L.; Harrington, P. B. *Anal. Chem.* **2004**, *76*, 985-991.

7. Rearden, P.; Harrington, P. B. *Anal. Chim. Acta* **2005**, *545*, 13-20.

8. Kaur-Atwal, G.; O'Connor, G.; Aksenov, A. A.; Bocos-Bintintan, V.; Thomas, C. L. P.; Creaser, C. S. *Int. J. Ion Mobil. Spec.* **2009**, *12*, 1-14.

9. Clemmer, D. E.; Jarrold, M. F. *J. Mass Spectrom.* **1997**, *32*, 577-592.

10. Hauck, B. C.; Davis, E. J.; Clark, A. E.; Siems, W. F.; Harden, C. S.; McHugh, V. M.; Hill, H. H., Jr. *Int. J. Mass Spectrom.* **2014**, *368*, 37-44.

11. Hauck, B. C.; Siems, W. F.; Harden, C. S.; McHugh, V. M.; Hill, H. H., Jr. *Rev. Sci. Instrum.* **2016**, *87*, 075104.

12. Hauck, B. C. *High Accuracy Ion Mobility Spectrometry to Reduce False Alarm Rates in National Security Technology*. Ph.D. Thesis, Washington State University **2016**.

13. Davis, E. J.; Clowers, B. H.; Siems, W. F.; Hill, H. H., Jr. *Int. J. Ion Mobil. Spec.* **2011**, *14*, 117-124.

14. Crawford, C. L.; Hauck, B. C.; Tufariello, J. A.; Harden, C. S.; McHugh, V.; Siems, W. F.; Hill, H. H., Jr. *Talanta* **2012**, *101*, 161-170.